THE JOURNAL OF PHYSICAL CHEMISTRY C

Article

Cite This: J. Phys. Chem. C 2018, 122, 7670−7675

pubs.acs.org/JPCC

First-Principles Screening of All-Inorganic Lead-Free ABX_3 Perovskites

Xin Mao,[†,‡] Lei Sun,[†] Tao Wu,[†] Tianshu Chu,[†] Weiqiao Deng,*[,†] and Keli Han*[,†,§]

[†]State Key Laboratory of Molecular Reaction Dynamics, Dalian Institute of Chemical Physics, Chinese Academy of Sciences, Dalian 116023, People's Republic of China

[‡]University of the Chinese Academy of Sciences, Beijing 100039, People's Republic of China

[§]Institute of Molecular Sciences and Engineering, Shandong University, Qingdao 266000, People's Republic of China

Supporting Information

ABSTRACT: In order to address an all-inorganic halide lead-free perovskite for potential photovoltaic applications, we carried out first-principles calculations of bandgaps of 260 all-inorganic halide perovskites belonging to the class ABX_3, with A = Li, Na, K, Rb, Cs, B = Pb, Sn, and Ge, and X = F, Cl, Br, I. Three most common crystal symmetries were chosen, including cubic, tetragonal, and two orthorhombic phases. The bandgap exhibited increase with the decreasing of the anions radius (I, Br, Cl, F) and lowering the symmetry of the structures. With consideration of multiple factors forming perovskites, we reported three all-inorganic lead-free halides perovskites including cubic-$KSnCl_3$, cubic-$RbSnCl_3$, and trigonal-$NaGeBr_3$ as candidates with desirable bandgap (1.24−1.44 eV) for photovoltaic applications.

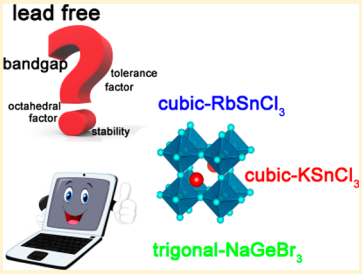

In the past few years, halide perovskites ABX_3 have received a revival of interest as potential photovoltaic materials due to the easily fabricated techniques and outstanding optoelectronic properties, such as high absorption coefficient, proper bandgap, balanced electron and hole mobility, and low intrinsic recombination rates.[1−9] Although the power conversion efficiency of perovskite solar cells has leapt from 3.8% to exciting values, e.g., 22.1% for formamidinium lead iodide ($FAPbI_3$),[10−18] there are still some issues limiting their commercialization. The key concerns are the inherent toxicity of lead element and instability of organic−inorganic halide perovskites under humidity conditions due to the loose chemical bonding of the related organic cations.[19−21] It is clear that future energy scenario demands nontoxic and stable perovskite materials, e.g., all-inorganic lead-free perovskites. Both Sn(II) and Ge(II) from the same group of periodic table with Pb(II) are considered to be primary candidates replacing the lead due to their similar electronic properties. However, the present efficiency of Sn-based, Ge-based all-inorganic perovskite solar cell is low, e.g., 0.2% for $CsGeI_3$, 3.31% for $CsSnI_3$, and far from desirable values.[22−24] Hence seeking new all-inorganic lead-free perovskite is still on the way.

In this aspect, computational simulation is used as a feasible and low-cost approach for materials screening. In particular, the method DFT-GLLB-SC has been recently tested against the many-body perturbation method based on Green's functional and experiments for perovskite materials and shown to give reasonable bandgaps at a minimal cost.[25−28] Herein we focused on the bandgap factor with the consideration of structural stability for high-throughput screening of Sn-based, Ge-based all-inorganic perovskites for photovoltaic application. The bandgaps of 260 all-inorganic halide perovskites ABX_3 (Figure 1) with different crystal phases were investigated by first-principle calculations with the method DFT-GLLB-SC in

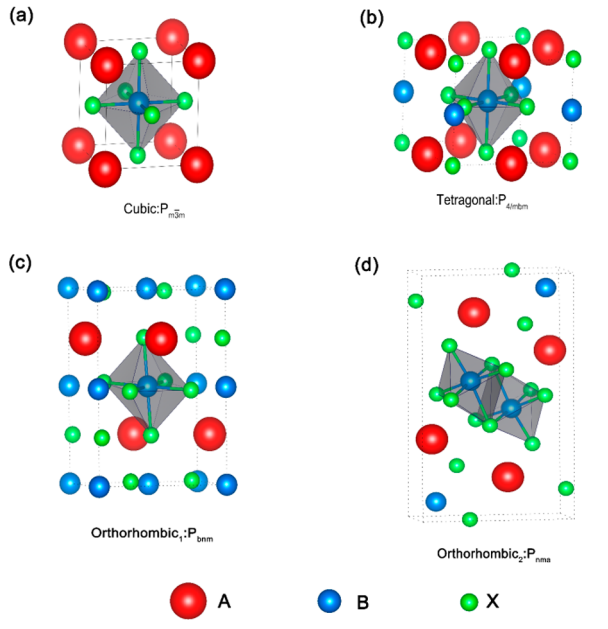

Figure 1. Crystal structures ABX_3 studied in this work: (a) cubic; (b) tetragonal; (c, d) the two orthorhombic. A cations contain Li^+, Na^+, K^+, Rb^+, and Cs^+. B cations are composed of Ge^{2+}, Sn^{2+}, and Pb^{2+}. And I^-, Br^-, Cl^-, F^- are used as the X anions.

Received: March 13, 2018
Published: March 20, 2018

DOI: 10.1021/acs.jpcc.8b02448
J. Phys. Chem. C 2018, 122, 7670−7675

consideration of spin−orbital coupling (SOC). Among them, A represents one of cesium (Cs^+), lithium (Li^+), sodium (Na^+), potassium (K^+), and rubidium (Rb^+) ; B represents one of tin (Sn^{2+}), germanium (Ge^{2+}), and lead (Pb^{2+}), and fluorine (F^-), chlorine (Cl^-), bromine (Br^-), iodine (I^-) are used as anions X_3^{3-}. We selected the three most common symmetries, including cubic, tetragonal, and two orthorhombic phases.[27] Furthermore, the $AGeX_3$ with the trigonal symmetry is also in consideration.[24]

First, to verify the bandgap calculation accuracy of the method used in this work, the bandgaps of a set of selected halide perovskites where the crystal structure is well determined, e.g., $CsPbCl_3$ and $CH_3NH_3GeI_3$, are calculated and shown in Table 1. Compared to the general Kohn−Sham bandgap, the calculated bandgap shows better agreement with those of experiments, in particular for cubic $CH_3NH_3PbI_3$, indicating good reliability of the method used in this work.

Table 1. Bandgap Comparison between Calculated (E_g) and Experimental Gaps (E_g^{exp}) of Selected Halide Perovskites (in eV)[a]

compound	phase	E_g^{exp}	E_g	E_{gap}^{KS}	Δ_{xc}	Δ_{SOC}
$CsPbCl_3$	tetragonal	2.86[29]	2.84	2.89	1.07	1.12
$CsGeI_3$	trigonal	1.63[24]	1.56	1.19	0.50	0.13
$CH_3NH_3PbI_3$	cubic	1.52[30]	1.56	1.82	0.75	1.01
$CH_3NH_3GeI_3$	trigonal	2.00[24]	1.83	1.37	0.58	0.13
$CsGeBr_3$	trigonal	2.32[31]	2.27	1.67	0.65	0.05

[a]Kohn−Sham bandgap E_{gap}^{KS}, exchange−correlation energy Δ_{xc} and spin-orbit coupling Δ_{SOC} are also listed.

EACH COLORED SQUARE CORRESPONDS TO A DIFFERENT COMPOSITION AND PHASE

The calculated bandgaps of 240 all-inorganic halide perovskites with symmetries containing cubic, tetragonal, and two orthorhombic phases are shown in Figure 2. The bandgaps span over a range from around 0.5 to around 7.0 eV. It is notable that the bandgaps of selected perovskites increase when X part changes from I, Br, Cl to F (from left to right for each ABX_3 with the same symmetry). The bandgaps also increase with the lowering the symmetry of the structure (from the bottom to the top of the plot for each A-ion). Generally, the color becomes brighter from $ASnX_3$ to $AGeX_3$ to $APbX_3$ in each row, which indicates the trend in bandgap is $ASnX_3$ < $AGeX_3$ < $APbX_3$ with the same symmetry. Different from the previous work, there is no obvious rule on effect of A cations in the same crystal phase.[27] To further reveal the factors controlling the bandgap trends, density of states (DOS) and partial density of states (PDOS) based on variable control approach were carried out.

First, to study the effect of B cations on bandgap trend, DOS and PDOS of three cubic perovskites, $CsGeBr_3$, $CsSnBr_3$, and $CsPbBr_3$ were calculated and shown in Figure 3. It is obvious that Cs does not contribute to the basic electronic structures.

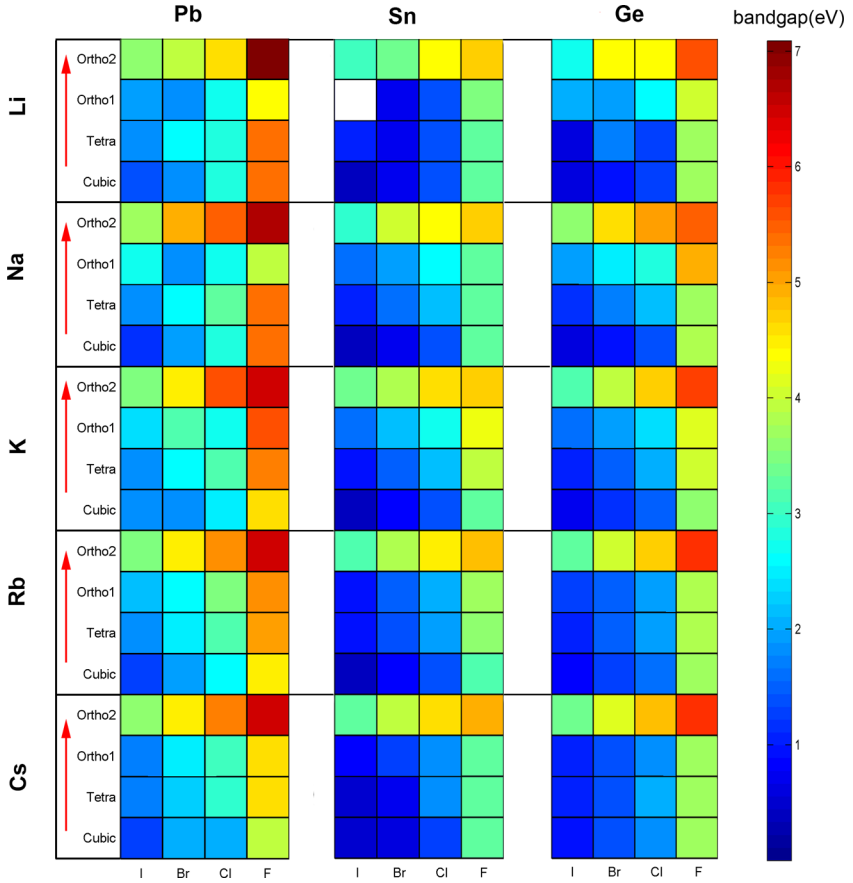

Figure 2. Calculated bandgaps (eV) of perovskite structures in this work. Corresponding A cations are listed on the left, while different B cations are listed on top by each column, and X anions are listed below. Corresponding to each A cation, from bottom to top, the crystal symmetry is reduced. The optimization of orthorhombic$_1$-$LiSnI_3$ does not converge.

DOI: 10.1021/acs.jpcc.8b02448
J. Phys. Chem. C 2018, 122, 7670−7675

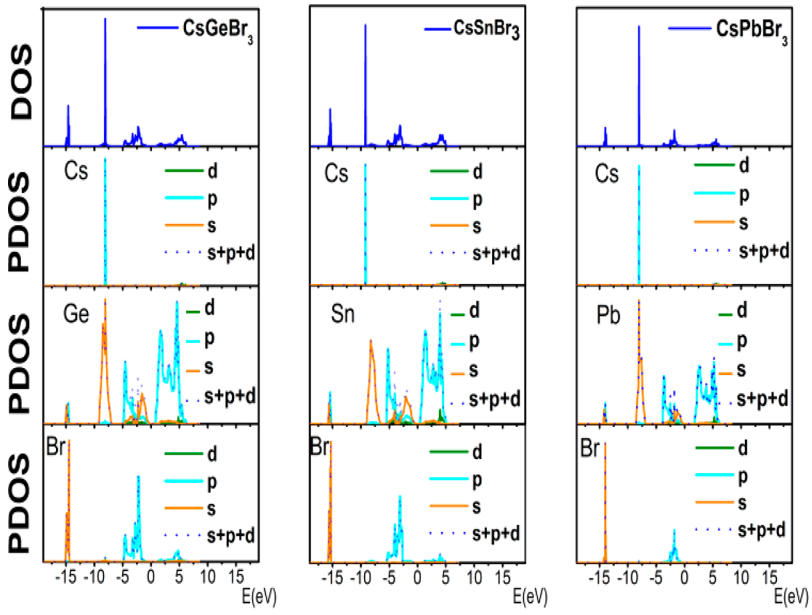

Figure 3. Density of states (DOS) and partial density of states (PDOS) using DFT-PBE calculations: (a) cubic-$CsGeBr_3$, (b) cubic-$CsSnBr_3$, (c) cubic-$CsPbBr_3$.

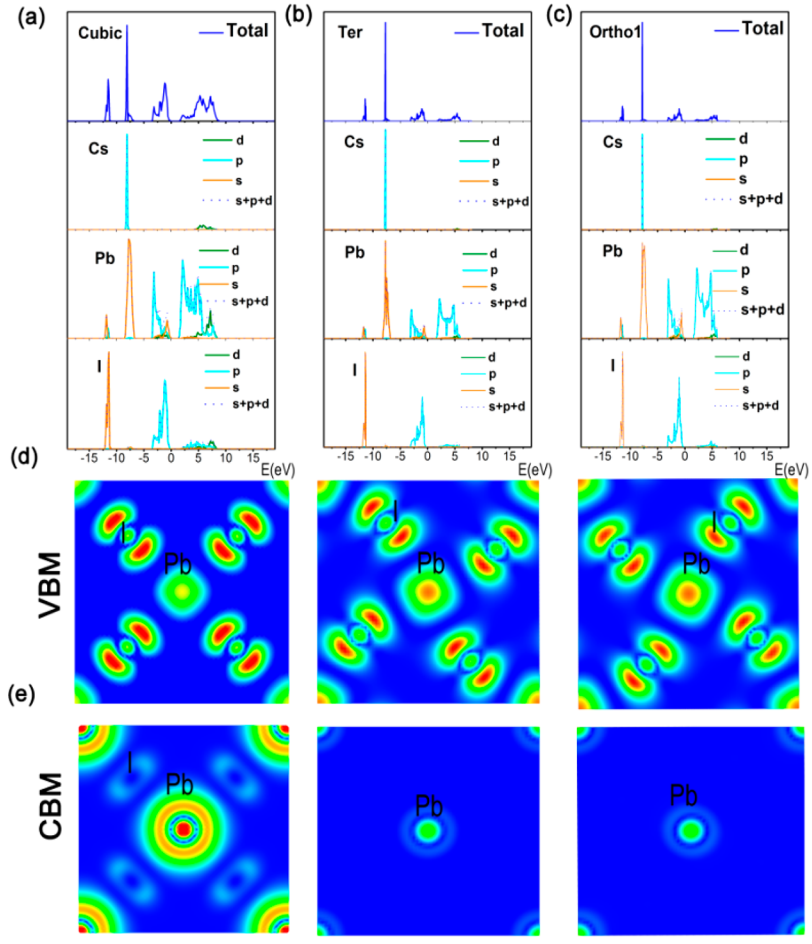

Figure 4. (a–c) Density of states and partial density of states of Cubic-$CsPbI_3$, tetragonal-$CsPbI_3$, and ortho$_1$-$CsPbI_3$. (d, e) VBM and CBM-associated charge density maps on the (001) plane for the cubic-$CsPbI_3$, Ter-$CsPbI_3$ and ortho$_1$-$CsPbI_3$(from left to right).

The valence band maximum (VBM) is derived from the p orbitals of Br and s orbitals of B, and their overlapping indicates the significant hybridization. The p orbitals of B and a bit of p orbitals of Br constitute the conduction band minimum (CBM). The trend of difference value between VBM and

DOI: 10.1021/acs.jpcc.8b02448
J. Phys. Chem. C 2018, 122, 7670−7675

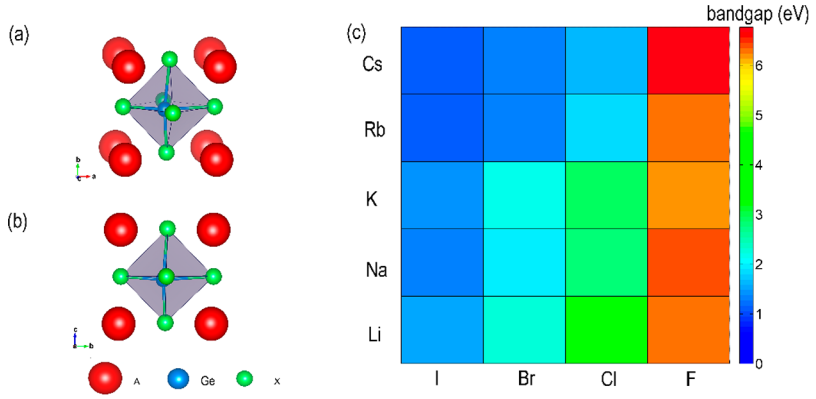

Figure 5. Crystal structure trigonal-$AGeX_3$ studied in this work: (a) unit cell; (b) top view of the unit cell. (c) The bandgap is shown with different colors (in eV). The left shows the A cation, while the bottom shows the X anions.

CBM for cubic-$CsGeBr_3$, $CsSnBr_3$, and $CsPbBr_3$ is consistent with the change of calculated bandgaps.

Then, to reveal the relationship between crystal symmetries and bandgaps, DOS, PDOS and CBM, VBM associated with charge density maps on the (001) plane of $CsPbI_3$ with three different symmetries, cubic, tetragonal, and orthorhombic$_1$ are calculated and shown in Figure 4. The orthorhombic$_2$ structure is not in consideration because the face-sharing octahedral owns too large bandgap which is not suitable for photovoltaic application. As show in Figure 4a–d, the VBM consists of s orbital of Pb and p orbital of I. When symmetry changes from cubic to orthorhombic$_1$, the angle θ of Pb–I–Pb varies from 180° to 153°. For the orthorhombic$_1$ $CsPbI_3$ with θ = 153°, the I atom is not at the center of the two neighboring Pb atoms, reducing the in-plane antibonding orbital overlap of Pb 6s–I 5p which attributes to the lower energy in VBM. Furthermore, the distortions of the lattice significantly decrease the contribution of Px and Py to the CBM as shown in Figure 4e, leading to small increase of energy of CBM. Similar results have also been reported by Yan et al.[32]

Given that the stable crystal symmetry of Ge-perovskite is trigonal at room temperature, additional 20 Ge-based perovskites were in consideration.[24] The Ge ion is too small, not at the center of the unit cell, leading to distortion of the lattice as shown in Figure 5. The bandgap trend is accordance with the results of 240 perovskites as discussed above.

The spin–orbit coupling (SOC) also plays an important role on the bandgap. As shown in Table S1 in Supporting Information, the Δsoc increases with the increasement of the symmetry of the structure and the mass of the B cations. In addition, from I anions to F anions, the Δsoc gradually decreases.

The effective mass of the carriers is an important index of the transport property of photovoltaic materials. B cations, X anions, and the symmetries of perovskite structure play an important role in determining the effective mass of the carriers. Tian[33] and her co-workers point out that the effective mass for electrons and holes perovskites (ABX_3) with the same part A and part B becomes smaller from $CsSnCl_3$ (0.28:0.09), $CsSnBr_3$ (0.22:0.06) to $CsSnI_3$ (0.17:0.04) and from $CsPbF_3$ (0.45:0.26), $CsPbCl_3$ (0.28:0.18) to $CsPbBr_3$ (0.22:0.14). And the effective masses for holes of Sn perovskites are smaller than those of Ge and Pb perovskites, resulting in the higher hole mobility of Sn perovskites. Liu et al.[34] find the effective mass of electrons and holes increase with the lowering of the symmetry of the structure from tetragonal $CH_3NH_3PbI_3$ to orthorhombic $CH_3NH_3PbI_3$.

According to the Shockley–Queisser (S-Q) detailed-balance model, the optimum semiconductor band gap for high photovoltaic energy conversion efficiency is 1.34 eV.[35] Herein we set the bandgap range 1.24 eV $\leq E_g \leq$ 1.44 eV as selection criteria. On the basis of Goldschmidt's rule, the ionic radius of A, B, and X need to meet the condition of the tolerance factor: $0.8 < t < 1$. The radiuses of the A, B cations and X anions are presented in Table S2. And the octahedral factor (μ) given by R_B/R_X should be within the range from 0.414 to 0.732 for perovskite formation.[15] Taking the factors including bandgaps, octahedral, and the tolerance factors into account, we selected three candidates, cubic $KSnCl_3$, cubic $RbSnCl_3$, and trigonal $NaGeBr_3$ from the lead-free perovskites as shown in Table 2.

Table 2. Summary of the Related Parameters Including Phase Group, Bandgap, Tolerance Factor (t), Octahedral Factor (μ), and Formation Energy of the Selected Lead-Free Perovskites

candidate	phase group	bandgap (eV)	t	μ	formation energy (eV/atom)
$KSnCl_3$	cubic	1.37 (direct)	0.83	0.51	0.010
$RbSnCl_3$	cubic	1.43 (direct)	0.86	0.51	−0.037
$NaGeBr_3$	trigonal	1.33 (direct)	0.78	0.37	0.142

Furthermore, to discuss the stability of these candidates, their formation energies are calculated, and all of them meet the criterion ΔE < 0.2 eV/atom which is adopted in the previous work.[36] The tolerance and octahedral factors of trigonal $NaGeBr_3$ are 0.78 and 0.37, respectively, approaching the limit values. For cubic $KSnCl_3$ and $RbSnCl_3$, their tolerance and octahedral factors fulfill the screening criteria. The calculated bandgap of cubic-$RbSnCl_3$ is close to Sabine's work,[37] which further proves the reasonableness of the method used in this work. To the best of our knowledge, the predicted three candidates, cubic $KSnCl_3$, cubic $RbSnCl_3$, and trigonal $NaGeBr_3$ have not been synthesized experimentally up to now and more work needs to be done.

In summary, we performed DFT-GLLB-SC calculations on 260 all-inorganic halide inorganic perovskites with different crystal phases to investigate their bandgaps for selecting candidates for applications in photovoltaic field. With the

DOI: 10.1021/acs.jpcc.8b02448
J. Phys. Chem. C 2018, 122, 7670–7675

combination of DOS and charge maps, the factors corresponding to the bandgap change are revealed. Both B-cations and crystal symmetry play an important role in determining the bandgap. The Ge-based halide perovskite was studied with the method DFT-GLLB-SC for the first time. Three unexplored all-inorganic lead-free halide perovskites cubic-$KSnCl_3$, cubic-$RbSnCl_3$, and trigonal-$NaGeBr_3$ have been screened out as candidate materials for photovoltaic applications.

COMPUTATIONAL METHODS

In this study, all structure optimizations are calculated by the generalized gradient approximation (GGA) with density functional theory (DFT) implemented in the Vienna ab initio simulation package (VASP).[38,39]The interaction between electron and ion is described by the projector-augmented wave method (PAW),[40] while the Perdew−Burke−Ernzerhof (PBE)[41] functional is applied to describe the electron exchange correlation. The cutoff energy is 400 eV, and the convergence threshold for self-consistent field (SCF) is 10^{-4} eV, while the atomic positions were fully optimized until all components of the residual forces were smaller than 0.02e V/Å. The Monkhorst−Pack k point sampling used in our calculation is $7 \times 7 \times 7$ for cubic and $7 \times 7 \times 7$ for tetragonal, $11 \times 7 \times 11$ for orthorhpmbic$_1$, and $8 \times 5 \times 20$ for orthorhpmbic$_2$. We use the GLLB-SC model potential method implemented in GPAW code[42−45] to predict the bandgaps of all the optimized perovskite structures. The GLLB-SC functional by Gritsenko, van Leeuwen, van Lenthe, and Baerends (GLLB),[44] adapted by Kuisma et al.[45] to include the PBEsol correlation for solids (-SC) has been tested with other computational methods (mainly of G_0W_0) and experiment values and shown to give reasonable results at a low cost.[25−28] In this method, excess exchange−correlation energy (Δ_{xc}) is considered based on Kohn−Sham bandgap to obtain the quasiparticle bandgap which includes two parts: Kohn−Sham bandgap $E_{gap}^{KS}$and exchange−correlation energy Δ_{xc}. Besides, for accurate description of bandgaps, spin−orbit coupling (SOC) calculations are also considered in our calculation as Δ_{SOC} which can be obtained from the VASP calculation.

$$E_g = E_{gap}^{KS} + \Delta_{xc} - \Delta_{soc}$$

ASSOCIATED CONTENT

Supporting Information

The Supporting Information is available free of charge on the ACS Publications website at DOI: 10.1021/acs.jpcc.8b02448.

Detailed calculated bandgap results for 262 perovskites studied in this work, radiuses of ions of ABX_3 perovskites studied in this work, and space groups of compounds used for formation energy calculations (PDF)

AUTHOR INFORMATION

Corresponding Authors

*W.-Q.D.: e-mail, dengwq@dicp.ac.cn.

*K.-l.H.: e-mail, klhan@dicp.ac.cn.

ORCID

Tao Wu: 0000-0001-9543-0377

Weiqiao Deng: 0000-0002-3671-5951

Keli Han: 0000-0001-9239-1827

Notes

The authors declare no competing financial interest.

ACKNOWLEDGMENTS

This work was supported by the National Natural Science Foundation of China (Grants 21533010 and 21403211), the National Key Research and Development Program of China (Grant 2017YFA0204800), Grant DICP DMTO201601, Grant DICP ZZBS201703, and the Science Challenging Program (Grant JCKY2016212A501).

REFERENCES

(1) Im, J. H.; Lee, C. R.; Lee, J. W.; Park, S. W.; Park, N. G. 6.5% Efficient perovskite quantum-dot-sensitized solar cell. *Nanoscale* **2011**, *3*, 4088−4093.

(2) Wehrenfennig, C.; Eperon, G. E.; Johnston, M. B.; Snaith, H. J.; Herz, L. M. High Charge Carrier Mobilities and Lifetimes in Organolead Trihalide Perovskites. *Adv. Mater.* **2014**, *26*, 1584−1589.

(3) Green, M. A.; Ho-Baillie, A.; Snaith, H. J. The Emergence of Perovskite Solar Cells. *Nat. Photonics* **2014**, *8*, 506−514.

(4) Stranks, S. D.; Snaith, H. J. Metal-Halide Perovskites for Photovoltaic and Light-Emitting Devices. *Nat. Nanotechnol.* **2015**, *10*, 391−402.

(5) Gao, P.; Gratzel, M.; Nazeeruddin, M. K. Organohalide Lead Perovskites for Photovoltaic Applications. *Energy Environ. Sci.* **2014**, *7*, 2448−2463.

(6) Correa-Baena, J. P.; Abate, A.; Saliba, M.; Tress, W.; Jesper Jacobsson, T.; Gratzel, M.; Hagfeldt, A. The Rapid Evolution of Highly Efficient Perovskite Solar Cells. *Energy Environ. Sci.* **2017**, *10*, 710−727.

(7) Zhao, Y.; Zhu, K. Organic−Inorganic Hybrid Lead Halide Perovskites for Optoelectronic and Electronic Applications. *Chem. Soc. Rev.* **2016**, *45*, 655−689.

(8) Sum, T. C.; Mathews, N. Advancements in Perovskite Solar Cells: Photophysics Behind the Photovoltaics. *Energy Environ. Sci.* **2014**, *7*, 2518−2534.

(9) Habibi, M.; Zabihi, F.; Ahmadian-Yazdi, M. R.; Eslamian, M. Progree in emerging solution-processed thin film solar cells-Part II: Perovskite solar cells. *Renewable Sustainable Energy Rev.* **2016**, *62*, 1012.

(10) Yang, W. S.; Park, B.-W.; Jung, E. H.; Jeon, N. J.; Kim, Y. C.; Lee, D. U.; Shin, S. S.; Seo, J.; Kim, E. K.; Noh, J. H.; et al. Iodide Management in Formamidinium-Lead-Halide-Based Perovskite Layers for Efficient Solar Cells. *Science* **2017**, *356*, 1376−1379.

(11) Yang, W. S.; Noh, J. H.; Jeon, N. J.; Kim, Y. C.; Ryu, S.; Seo, J.; Seok, S. I. High-performance photovoltaic perovskite layers fabricated through intramolecular exchange. *Science* **2015**, *348*, 1234−1237.

(12) Bi, D.; Tress, W.; Dar, M. I.; Gao, P.; Luo, J.; Renevier, C.; Schenk, K.; Abate, A.; Giordano, F.; Correa Baena, J.-P.; et al. Efficient Luminescent Solar Cells Based on Tailored Mixed-Cation Perovskites. *Sci. Adv.* **2016**, *2*, e1501170.

(13) Momblona, C.; Gil-Escrig, L.; Bandiello, E.; Hutter, E. M.; Sessolo, M.; Lederer, K.; Blochwitz-Nimoth, J.; Bolink, H. J. Efficient Vacuum Deposited P-I-N and N-I-P Perovskite Solar Cells Employing Doped Charge Transport Layers. *Energy Environ. Sci.* **2016**, *9* (11), 3456−3463.

(14) Anaraki, E. H.; Kermanpur, A.; Steier, L.; Domanski, K.; Matsui, T.; Tress, W.; Saliba, M.; Abate, A.; Grätzel, M.; Hagfeldt, A.; et al. Highly Efficient and Stable Planar Perovskite Solar Cells by Solution-Processed Tin Oxide. *Energy Environ. Sci.* **2016**, *9* (10), 3128−3134.

(15) Saliba, M.; Matsui, T.; Domanski, K.; Seo, J. Y.; Ummadisingu, A.; Zakeeruddin, S. M.; Correa-Baena, J.-P.; Tress, W. R.; Abate, A.; Hagfeldt, A.; Gratzel, M. Incorporation of Rubidium Cations Into Perovskite Solar Cells Improves Photovoltaic Performance. *Science* **2016**, *354*, 206−209.

(16) Tan, H.; Jain, A.; Voznyy, O.; Lan, X.; García de Arquer, F. P.; Fan, J. Z.; Quintero-Bermudez, R.; Yuan, M.; Zhang, B.; Zhao, Y.; et al. Efficient and Stable Solution-Processed Planar Perovskite Solar Cells via Contact Passivation. *Science (Washington, DC, U. S.)* **2017**, *355*, 722−726.

DOI: 10.1021/acs.jpcc.8b02448
J. Phys. Chem. C 2018, 122, 7670−7675

(17) Shin, S. S.; Yeom, E. J.; Yang, W. S.; Hur, S.; Kim, M. G.; Im, J.; Seo, J.; Noh, J. H.; Seok, S. I. Colloidally prepared La-doped $BaSnO_3$ electrodes for efficient, photostable perovskite solar cells. *Science* **2017**, *356*, 167−171.
(18) Stolterfoht, M.; Wolff, C. M.; Amir, Y.; Paulke, A.; Perdigón-Toro, L.; Caprioglio, P.; Neher, D. Approaching the fill factor Shockley−Queisser limit in stable, dopant-free triple cation perovskite solar cells. *Energy Environ. Sci.* **2017**, *10*, 1530−1539.
(19) Sutton, R. J.; Eperon, G. E.; Miranda, L.; Parrott, E. S.; Kamino, B. A.; Patel, J. B.; Hörantner, M. T.; Johnston, M. B.; Haghighirad, A. A.; Moore, D. T.; et al. Bandgap-tunable cesium lead halide perovskites with high thermal stability for efficient solar cells. *Adv, Ener. Mater.* **2016**, *6*, 1502458.
(20) Niu, G.; Guo, X.; Wang, L. Review of Recent Progress in Chemical Stability of Perovskite Solar Cells. *J. Mater. Chem. A* **2015**, *3*, 8970−8980.
(21) Kulbak, M.; Cahen, D.; Hodes, G. How important is the organic part of lead halide perovskite photovoltaic cells? Efficient CsPbBr3 cells. *J. Phys. Chem. Lett.* **2015**, *6*, 2452−2456.
(22) Shi, Z.; Guo, J.; Chen, Y.; Li, Q.; Pan, Y.; Zhang, H.; Xia, Y.; Huang, W. Lead-Free Organic−Inorganic Hybrid Perovskites for Photovoltaic Applications: Recent Advances and Perspectives. *Adv. Mater.* **2017**, *29*, 1605005.
(23) Wang, N.; Zhou, Y.; Ju, M.; Garces, H. F.; Ding, T.; Pang, S.; Zeng, X. C.; Padture, N. P.; Sun, X. W. Heterojunction-depleted lead-free perovskite solar cells with coarse-grained B-γ-$CsSnI_3$ thin films. *Adv. Energ Mater.* **2016**, *6*, 1601130.
(24) Krishnamoorthy, T.; Ding, H.; Yan, C.; Leong, W. L.; Baikie, T.; Zhang, Z.; Sherburne, M.; Li, S.; Asta, M.; Mathews, N.; et al. Lead-Free Germanium Iodide Perovskite Materials for Photovoltaic Applications. *J. Mater. Chem. A* **2015**, *3*, 23829−23832.
(25) Li, Y.-J.; Wu, T.; Sun, L.; Yang, R.-X.; Jiang, L.; Cheng, P.-F.; Hao, Q.-Q.; Wang, T.-J.; Lu, R.-F.; Deng, W.-Q. Lead-free and stable antimony-silver-halide double perovskite $(CH_3NH_3)_2AgSbI_6$. *RSC Adv.* **2017**, *7*, 35175−35180.
(26) Pandey, M.; Jacobsen, K. W.; Thygesen, K. S. Band Gap Tuning and Defect Tolerance of Atomically Thin Two-Dimensional Organic-Inorganic Halide Perovskites. *J. Phys. Chem. Lett.* **2016**, *7*, 4346−4352.
(27) Castelli, I. E.; García-Lastra, J. M.; Thygesen, K. S.; Jacobsen, K. W. Bandgap Calculations and Trends of Organometal Halide Perovskites. *APL Mater.* **2014**, *2*, 081514.
(28) Castelli, I. E.; Hüser, F.; Pandey, M.; Li, H.; Thygesen, K. S.; Seger, B.; Jain, A.; Persson, K. A.; Ceder, G.; Jacobsen, K. W. New Light-Harvesting Materials Using Accurate and Efficient Bandgap Calculations. *Adv. Ener. Mater.* **2015**, *5*, 1400915.
(29) Ahmad, J.; Rehman, G.; Ali, L.; Shafiq, M.; Iqbal, R.; Ahmad, R.; Khan, T.; Jalali-Asadabadi, S.; Maqbool, M.; Ahmad, I. Structural, electronic and optical properties of $CsPbX_3$ (X = Cl, Br, I) for energy storage and hybrid solar cell applications. *J. Alloys Compd.* **2017**, *705*, 828−839.
(30) Eperon, G. E.; Stranks, S. D.; Menelaou, C.; Johnston, M. B.; Herz, L. M.; Snaith, H. J. Formamidinium Lead Trihalide: A Broadly Tunable Perovskite for Efficient Planar Heterojunction Solar Cells. *Energy Environ. Sci.* **2014**, *7*, 982−988.
(31) Seo, D.-K.; Gupta, N.; Whangbo, M.-H.; Hillebrecht, H.; Thiele, G. Pressure-induced changes in the structure and band gap of $CsGeX_3$ (X = Cl, Br) studied by electronic band structure calculations. *Inorg. Chem.* **1998**, *37*, 407−410.
(32) Xiao, Z.; Meng, W.; Wang, J.; Mitzi, D. B.; Yan, Y. Searching for Promising New Perovskite-Based Photovoltaic Absorbers: the Importance of Electronic Dimensionality. *Mater. Horiz.* **2017**, *4*, 206−216.
(33) Qian, J.; Xu, B.; Tian, W. A Comprehensive Theoretical Study of Halide Perovskites ABX_3. *Org. Electron.* **2016**, *37*, 61−73.
(34) Geng, W.; Zhang, L.; Zhang, Y.-N.; Lau, W.-M.; Liu, L.-M. First-principles Study of Lead Iodide Perovskite Tetragonal and Orthorhombic Phases for Photovoltaics. *J. Phys. Chem. C* **2014**, *118*, 19565−19571.
(35) Polman, A.; Knight, M.; Garnett, E. C.; Ehrler, B.; Sinke, W. C. Photovoltaic materials: Present efficiencies and future challenges. *Science* **2016**, *352*, aad4424.
(36) Castelli, I. E.; Olsen, T.; Datta, S.; Landis, D. D.; Dahl, S.; Thygesen, K. S.; Jacobsen, K. W. Computational Screening of Perovskite Metal Oxides for Optimal Solar Light Capture. *Energy Environ. Sci.* **2012**, *5*, 5814−5819.
(37) Körbel, S.; Marques, M. A.; Botti, S. Stability and Electronic Properties of New Inorganic Perovskites from High-Throughput Ab Initio Calculations. *J. Mater. Chem. C* **2016**, *4*, 3157−3167.
(38) Kresse, G.; Furthmüller, J. Efficient Iterative Schemes for ab initio Total-energy Calculations Using a Plane-wave Basis Set. *Phys. Rev. B: Condens. Matter Mater. Phys.* **1996**, *54*, 11169−11186.
(39) Kresse, G.; Furthmüller, J. Efficiency of ab-initio total energycalculations for metals and semiconductors using a plane-wave basisset. *Comput. Mater. Sci.* **1996**, *6*, 15−50.
(40) Blöchl, P. E. Projector Augmented-Wave Method. *Phys. Rev. B: Condens. Matter Mater. Phys.* **1994**, *50*, 17953.
(41) Perdew, J. P.; Burke, K.; Ernzerhof, M. Generalized Gradient Approximation Made Simple. *Phys. Rev. Lett.* **1996**, *77*, 3865.
(42) Mortensen, J. J.; Hansen, L. B.; Jacobsen, K. W. Real-space Grid Implementation of the Projector Augmented Wave Method. *Phys. Rev. B: Condens. Matter Mater. Phys.* **2005**, *71*, 035109.
(43) Enkovaara, J.; Rostgaard, C.; Mortensen, J. J.; Chen, J.; Du łak, M.; Ferrighi, L.; Gavnholt, J.; Glinsvad, C.; Haikola, V.; Hansen, H. A.; et al. Electronic structure calculations with GPAW: a real-space implementation of the projector augmented-wave method. *J. Phys.: Condens. Matter* **2010**, *22*, 253202.
(44) Gritsenko, O.; Van Leeuwen, R.; Van Lenthe, E.; Baerends, E. J. Self-consistent approximation to the kohn-sham exchange potential. *Phys. Rev. A: At., Mol., Opt. Phys.* **1995**, *51*, 1944−1954.
(45) Kuisma, M.; Ojanen, J.; Enkovaara, J.; Rantala, T. T. Kohn-Sham Potential with Discontinuity for Band Gap Materials. *Phys. Rev. B: Condens. Matter Mater. Phys.* **2010**, *82*, 115106.

DOI: 10.1021/acs.jpcc.8b02448
J. Phys. Chem. C 2018, 122, 7670−7675